Available online at www.sciencedirect.com
SCIENCE DIRECT®
Biochimica et Biophysica Acta 1655 (2004) 13–28
BIOCHIMICA ET BIOPHYSICA ACTA
BBA
www.bba-direct.com

Review

Proton-coupled electron transfer: a unifying mechanism for biological charge transport, amino acid radical initiation and propagation, and bond making/breaking reactions of water and oxygen

Christopher J. Chang, Michelle C.Y. Chang, Niels H. Damrauer, Daniel G. Nocera*

Department of Chemistry, 6-335, 77 Massachusetts Avenue, Massachusetts Institute of Technology, Cambridge, MA 02139-4307, USA

Received 15 April 2003; accepted 8 August 2003

Abstract

Redox-driven proton pumps, radical initiation and propagation in biology, and small-molecule activation processes all involve the coupling of electron transfer to proton transport. A mechanistic framework in which to interpret these processes is being developed by examining proton-coupled electron transfer (PCET) in model and natural systems. Specifically, PCET investigations are underway on the following three fronts: (1) the elucidation of the PCET reaction mechanism by time-resolved laser spectroscopy of electron donors and acceptors juxtaposed by a proton transfer interface; (2) the role of amino acid radicals in biological catalysis with the radical initiation and transport processes of *E. coli* ribonucleotide reductase (RNR) as a focal point; and (3) the application of PCET towards small–molecule activation with emphasis on biologically relevant bond-breaking and bond-making processes involving oxygen and water. A review of recent developments in each of these areas is discussed.

Keywords: Proton-coupled electron transfer; Tyrosyl radical; Oxygen and water activation; Cytochrome *c* oxidase; Photosystem II; Ribonucleotide reductase; Monooxygenase; Catalase; Pacman; Hangman; Porphyrin; Hydrogen-bonding; Heme water channel; Dagwoods

1. Introduction

The coupling of protons and electrons is fundamental to mechanisms of biological energy conversion. Redox-driven proton pumps, radical initiation and transport in biology and small-molecule activation processes can involve the coupling of electron transfer to proton motion. Nowhere is this better demonstrated than for the enzymes in which Jerry Babcock (GTB) confronted the issue of proton-coupled electron transfer (PCET)—Photosystem II (PS II) and cytochrome *c* oxidase.

In GTB's initial studies, PCET was not manifested in a formal mechanistic framework; rather, it came in the guise of radicals. Although radical-based catalysis is now widely recognized as a common tool of the enzymatic arsenal [1], it should be noted that GTB, as a graduate student in Ken Sauer's group, was one of the first to recognize the importance of radicals in biology. At the time, he explored the mysterious EPR spectrum of "signal II" in PS II [2–7]. Penetrating EPR studies of subsequent years culminated with the recognition that the organic contributor to "signal II" was tyrosyl radical $^{\bullet}Y_Z$ (Y161 of the D1 polypeptide of PS II), which in turn was identified as the primary reductant of $P680^+$, the photoproduct of the specialized chlorophyll complex of PS II [8]. Following this discovery, one of us (DGN) had the pleasure of observing many delightful "group meetings" between GTB and Charlie Yocum at Dagwoods during which the importance of Y_Z in PS II came into focus. The dynamic between GTB and Charlie was intense and energizing. From these gatherings came the seminal proposal that Y_Z was the linchpin that managed electron and proton flow in the conversion of the primary light absorption event at the P680 chlorophylls into the multielectron activation of water at the oxygen-evolving complex (OEC) [9,10]. In short, every step of this transformation was proposed to involve a tightly coupled PCET event [11,12], as has been observed in model systems of the OEC complex [13]. Y_Z is deprotonated by a neighboring histidine (H191) as it

* Corresponding author. Tel.: +1-617-253-5537; fax: +1-617-253-7670.
E-mail address: nocera@mit.edu (D.G. Nocera).

0005-2728/$ - see front matter © 2004 Elsevier B.V. All rights reserved.
doi:10.1016/j.bbabio.2003.08.010

reduces $P680^+$ to form the neutral radical $\bullet Y_Z$, which in turn is the primary oxidant that steps the tetranuclear manganese cluster, one electron/one proton at a time, through each of the four S states of the Kok cycle [14], though the stoichiometry of electron and proton release has yet to be resolved definitively [15,16]. Structural support for this model has been provided by the ESEEM studies of Britt and co-workers, who have identified a tyrosine ideally situated between $P680^+$ and a $(3+1)$ $(Mn)_4$ cluster and in strong communication with specific manganese centers of the cluster [17].

The PCET chemistry of O_2 bond-forming at the $\bullet Y_Z$/OEC active site in PS II has remarkable chemical, mechanistic and structural similarities with the O_2 bond-breaking chemistry of the mammalian fuel cell, cytochrome *c* oxidase. It was GTB, again, who made this extraordinary insight in his BBA paper entitled "From Water to Oxygen and Back Again: Mechanistic Similarities in the Enzymatic Redox Conversions Between Water and Dioxygen" [18]. Fig. 1 pictorially summarizes the connection between photosynthesis and respiration. In GTB's construct of PS II, the "dimer-of-dimers" model is cited as the structure of the $(Mn)_4$ cluster [19]. At the time of this work, Britt's incisive ESEEM study in which the $(3+1)$ model was proposed [17] and the subsequent low-resolution X-ray structure of PS II [20] had not yet appeared in the literature; GTB would have surely modernized this scheme today with a $(Mn)_4$ $(3+1)$ active site. Notwithstanding, the essential elements of the scheme are retained, regardless of the precise structure of the $(Mn)_4$ cluster. Namely, a tyrosyl radical in PS II drives a series of PCET events that ultimately lead to a transient peroxo species, formed by the attack of a hydroxide on a metal oxo species. The transient peroxo species evolves O_2 upon further oxidation. In cytochrome *c* oxidase, the microscopic reverse was proposed: O_2 binding is followed by the formation of a transient peroxo, which undergoes a PCET reaction with the cross-linked tyrosyl radical to produce metal-oxo and hydroxo species.

Vestiges of the model in Fig. 1 began to be shaped by GTB in the early 1990s. During this time, DGN's days were frequently brightened by office visits from GTB, who came to learn particular details of inorganic chemistry that foreshadowed the mechanistic scheme of Fig. 1. (Another "inorganic advisor" to GTB over this same time period was Vince Pecoraro who figured prominently in shaping GTB's thinking about the chemistry of OEC). Dagwoods again was the ideal venue to continue early evening discussions late into the night. GTB's enthusiasm was infectious and he soon had us thinking more deeply about the intimate mechanistic details of bioenergy conversion. Significantly, interactions with GTB over this period prompted us to change the perspective from which we viewed the bioenergy problem. The inclination of an inorganic chemist is to start at the metal and dwell on redox chemistry as defined by Marcus and Taube; this course of thought invariably emphasizes the role of the electron in charge transport. On the other hand, GTB began at the radical and followed it into the metal cofactor active site. In doing so, energetic considerations involving tyrosine emphasized the proton and insisted upon its tight coupling to electron transport. It soon became obvious to us that the problem of electron coupled proton transfer was at the heart of three major issues encompassed in GTB's scheme of Fig. 1—charge transport (highlighted in red), tyrosyl radical relay (highlighted in green) and oxygen-oxygen bond breaking and bond making catalysis (highlighted in blue). Driven by these insights, a research program in PCET was created and

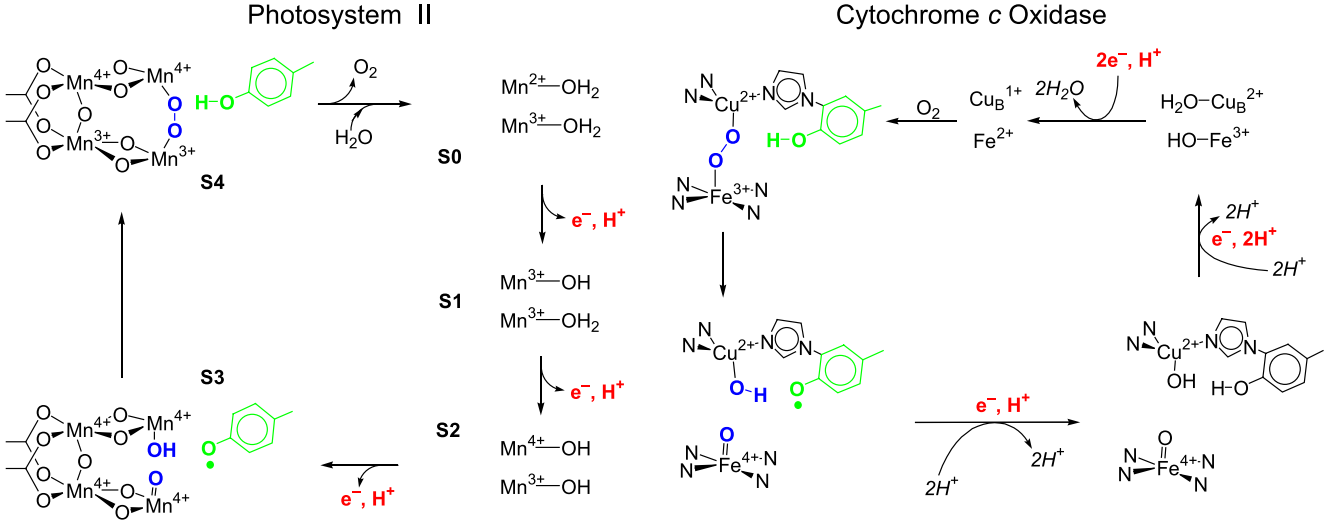

Fig. 1. The Babcock scheme for the PCET driven O_2 bond formation chemistry of PS II and O_2 bond cleavage chemistry of cytochrome *c* oxidase. Adapted from Ref. [18]. The tyrosyl radical is indicated in only the last step of the S cycle of PS II to emphasize the analogy with the reverse reaction catalyzed by cytochrome *c* oxidase.

developed along the following lines of inquiry: (1) a mechanistic description of PCET; (2) the role of PCET in biological charge transport, especially in radical transport among amino acids; and (3) the application of PCET towards biological small–molecule activation with emphasis on bond-making and bond-breaking processes involving oxygen. A review of our progress in each of these three areas is presented below.

2. Mechanistic studies of PCET

The coupling between the electron and the proton may be grouped into two general categories, which we designate as indirect and direct coupling. In the indirect coupling mechanism, electron and proton transport are driven by a thermodynamic gradient that is established by the flow of electrons prior to proton motion or vice versa. Here, the transport of an electron is not tied to a specific proton. A different situation arises for a direct coupling mechanism. The electron and the proton are linked to each other during transport. For this case, electron and proton movements do not need to be synchronous. As will be described below, the proton can affect the electron transport even when the electron and proton do not move together. Furthermore, the same electron and proton do not have to be coupled throughout an entire transformation. As the electron moves, it may encounter different protons along a transport chain. All that is required for direct coupling is that the kinetics (and thermodynamics) of electron transport depends on the position of a specific proton or set of protons at any given time. It is direct coupling of the electron and proton that is the most elementary characteristic of a PCET event.

Electron transfer (ET) provides a convenient starting point for the PCET problem. The ET rate constant is defined as,

$$k_{ET} = \frac{4\pi^2}{h} |V_{el}|^2 \times FCWD \quad (1)$$

where V_{el} is the magnitude of the electronic coupling and FCWD is the Franck-Condon weighted density of states, which accounts for the reaction free energy and reorganization energy as related by Marcus theory [21,22]. The PCET problem must account for the proton in addition to the electron. As the electron moves, the pK_as of redox cofactors change. Yet, knowledge of the driving force of the reaction alone is insufficient to predict kinetics. The FCWD factor will be affected by the charge redistribution resulting from electron and proton motion. In addition, the electronic coupling will change parametrically with the PT coordinate.

The need to treat both the proton and electron required the development of new experiments and theory. In response, PCET was launched at a mechanistic level with the approach shown in Fig. 2 [23,24]. In this scheme, PCET is photoinitiated between a donor (D) and an acceptor (A) juxtaposed by a hydrogen-bonding interface, [H^+]. The initial D–[H^+]–A construct exploited the propensity of carboxylic acids to form cyclic dimers ([H^+]=[$(COOH)_2$]) in low-polarity, non-hydrogen bonding solvents [25]. Measurement of the isotope effect for charge separation and recombination revealed the coupling between electron and proton. Within the –[$(COOH)_2$]– interface, proton displacement on one side of the dicarboxylic acid interface is compensated by the concomitant displacement of a proton from the other side. Because charge redistribution within this interface is

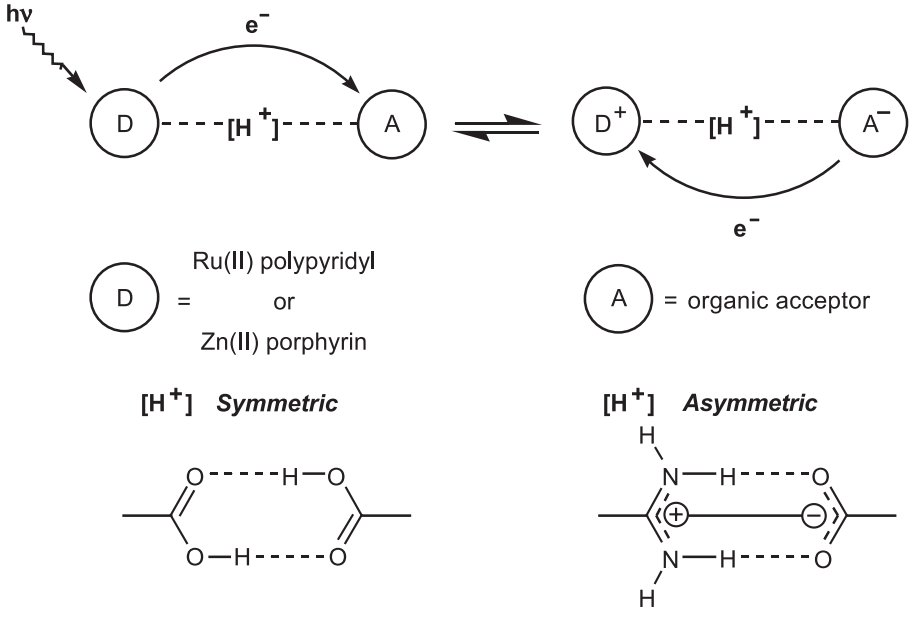

Fig. 2. Schematic representation of hydrogen-bonded donor–acceptor assemblies used for mechanistic investigations of PCET.

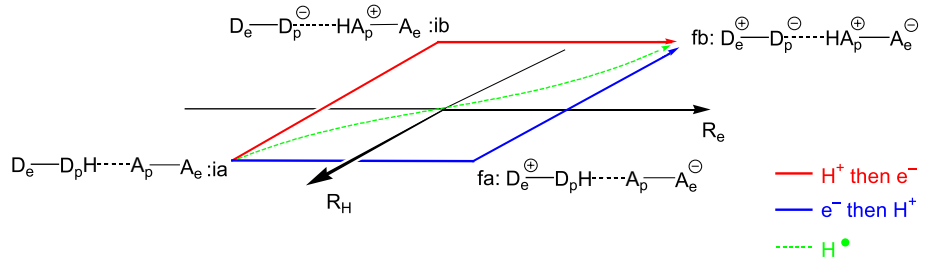

Fig. 3. PCET pathways. The blue line describes the transfer of the electron followed by the proton. The red line describes PT followed by ET. All other possible PCET pathways are confined within the space of the red and blue paths. One especially important pathway is along the diagonal. Here the electron and proton transfers are concerted—this corresponds to hydrogen atom transfer.

negligible, the only available mechanism for PCET arises from the dependence of the electronic coupling on the position of the protons within the interface [26–28]. Similar results have been obtained for donors and acceptors separated by guanine-cytosine base pairs [29–31] and related interfaces [32] where net proton motion within the interface is minimal. Yet such cases are unusual in Nature, where proton displacement almost always accompanies the redox process. Mechanistic studies were therefore expanded to include salt-bridge interfaces formed from the association of amidinium and carboxylate moieties [33–37]. The movement of a proton from the amidinium toward the carboxylate may accompany electron transfer from D to A. The effect of this proton motion on ET has been demonstrated by a comparative kinetics study of a D–[amidinium-carboxylate]–A complex and its inverted interfacial D–[carboxylate-amidinium]–A counterpart [33,37]. Differences between the charge transfer rate of the former is 10^2 slower than that of the latter.

A subsequent theoretical description of PCET [24,38] has developed around these data to explain the pronounced rate differences. Most treatments are based on the four-state model shown in Fig. 3: D_e is the electron donor, D_p is the proton donor, A_p is the proton acceptor and A_e is the electron acceptor. Fig. 3 illustrates the continuum of possible PCET reaction pathways. The initial state is {ia} and the final PCET state is {fb}. An ET with no proton transfer (PT) is described by {fa} whereas a PT with no ET is described by {ib}. The two zigzag ET/PT pathways describe (i) a change of the proton coordinate to an appropriate configuration after which ET occurs (red path: ia → ib → fb) or (ii) the transfer of an electron followed by the transfer of a proton (blue path: ia → fa → fb). The diagonal pathway describes a concerted PCET reaction, which chemically corresponds to a hydrogen atom transfer [39]. Historically, the definition of hydrogen atom transfer is often reserved for the situation where the proton and electron are transferred between the same donor and acceptor pair. However, we note that the diagonal pathway in Fig. 3 is completely general and does not distinguish between the sites of electron and proton transfer. Accordingly, a concerted electron and proton transfer is designated hydrogen atom transfer even if the electron donor and acceptor differ from the proton donor and acceptor. The challenging feature to developing a PCET theory is the disparate time scales for electron and proton motion; a proton is a much less quantum mechanical object than an electron due to its mass. To date, the time scale (or mass) separation between the electron and the proton has been treated by a Born–Oppenheimer separation of the proton from the electron. Under these conditions, the PCET rate constant is given by [24,38,40,41],

$$k_{\mathrm{PCET}} = H_{\mathrm{AD}}^2 \sqrt{\frac{4\pi^3}{h^2 \lambda_{\mathrm{PCET}} k_{\mathrm{B}} T}} \sum_{n'} \rho_{\mathrm{in}'} \sum_{n} |\langle \chi_{\mathrm{fn}} | \chi_{\mathrm{in}'} \rangle|^2 \times \exp\left[\frac{-(\lambda_{\mathrm{PCET}} + \Delta G^{\circ}_{\mathrm{PCET}} + \Delta \varepsilon_{n,n'})^2}{4 \lambda_{\mathrm{PCET}} k_{\mathrm{B}} T} \right] \quad (2)$$

where $\rho_{\mathrm{in}'}$ is a normalized Boltzmann factor accounting for the equilibrium distribution of the proton in the reactant well, with the electron in its initial state, i. In

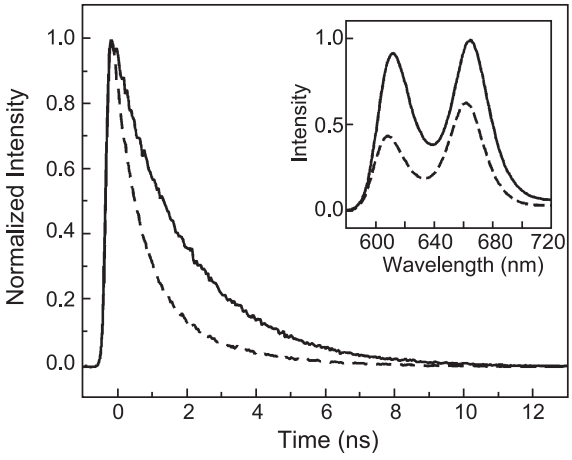

Fig. 4. Singlet (S_1) emission kinetics for a 6×10^{-5} M solution of the porphyrin donor chromophore alone in THF (solid) and following addition of two equivalents of the diimide acceptor (dashed). Emission was collected at 615 ± 5 nm following 407 nm/100 fs excitation. The inset shows static quenching of the emission spectrum for the porphyrin (50 μM) alone (solid) and after the addition of two equivalents of the acceptor (dashed).

Eq. (2), the electronic coupling of the ET problem is weighted by Franck-Condon factors connecting the proton in its initial and final state, $|\langle\chi_{fn}|\chi_{in'}\rangle|^2$. The proton also contributes to both parts of the FC term. The $\Delta\varepsilon_{n,n'}$ term accounts for the difference in vibrational energy levels for product and reactant states. Eq. (2) assumes that each pair of reactant and product states has the same reorganization energy and that the coupling can be expressed as the product of a constant electronic coupling and a proton vibrational overlap. A formal derivation of a more general PCET rate expression that does not make this assumption has been presented [38]. From these treatments of PCET, we find that the driving force and reorganization energy depend on the charge distribution of the electron and the proton because the initial and final charge values are dependent on whether the process corresponds to ET, PT or PCET. Therefore, the two parameters that determine the rate of a charge transfer reaction, the activation energy and the electronic coupling depend on the reaction pathway. The coupling of the charge shift resulting from electron *and* proton motion to the polarization of the surrounding environment is the essential distinguishing characteristic of a PCET reaction.

The desire to kinetically observe both the electron and proton transfer events has led us to develop new D–[H^+]–A systems whose PCET products are amenable to detection by transient spectroscopic methods. Our attention turned to synthesizing Zn(II) porphyrin donors with an amidinium functionality directly fused to the β and *meso* positions of the porphyrin ring [34,42]. In these systems, the porphyrin's B- and Q-bands can provide a spectroscopic handle for proton motion since these bands are sensitive to the protonation state of the amidine functionality when conjugated to the porphyrin macrocycle. The kinetics for ET may be monitored by following the time evolution of the porphyrin radical cation or of the reduced acceptor. With regard to the latter, we have bound Zn(II) porphyrin donors to naphthalene diimide acceptors functionalized with a carboxylate (**1**). The diimides are ideal acceptors for photoinitiated PCET studies because they display large ΔODs upon reduction in a spectral region that is not obscured by porphyrin absorption [43,44].

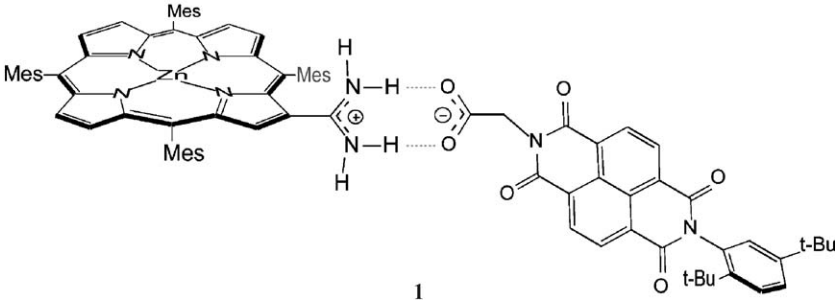

1

Assembly **1** and the unbound Zn(II) porphyrin have been investigated by transient absorption and emission methods [45]. As shown in Fig. 4, the S_1 excited state of the porphyrin is quenched considerably upon salt-bridge formation ($\tau = 2200$ ps for unbound porphyrin, $\tau(\mathbf{1}) = 720$ ps in THF, 25 °C). That this quenching occurs by PCET is established with the transient absorption spectroscopy. Transient features characteristic of the one-electron reduced diimide ($\Delta\varepsilon \sim 5000$ at 610 nm) as well as the porphyrin cation radical ($\Delta\varepsilon \sim$ 5000 at 660 nm) occur in the long wavelength region of the spectrum. Unfortunately, these spectral signatures cannot be easily observed because the coupling of electron to the proton significantly retards the charge transfer event. For this reason the yield of PCET products is low and consequently the spectral features of the reduced anion and Zn(II) porphyrin cation are overwhelmed by the dynamics of porphyrin S_1 and T_1 excited states. We have overcome this problem by performing single-wavelength kinetics at the S_1/T_1 isosbestic point ($\lambda_{probe} = 650$ nm). Fig. 5 (top) shows transient spectra collected for Zn(II) porphyrin at 500 ps, 1 ns and 2 ns. The small circle highlights the existence of the S_1/T_1 isosbestic point. At this wavelength the dynamics of the porphyrin excited states are effectively nulled; thus absorption features due to PCET products may therefore be detected against a "flat" background. These data are shown in Fig. 5 (bottom). The solid circles show the kinetics for the porphyrin donor in the absence of carboxylate acceptor. Because the probe is at an isosbestic point, the ΔOD does not change in time, and a step function is obtained. This simple transient behavior is perturbed dramatically upon addition of 2 equiv of the acceptor to form **1** ($K_{assoc} \sim 2 \times 10^4$). A clear rise time is observed for the growth of a transient absorption signal that is associated with the production of the porphyrin cation radical, followed by its subsequent decay. Kinetic analysis of the trace yield forward and back PCET rates of $k_{PCET} = 9.3 \times 10^8$ and 1.4×10^9 s^{-1}, respectively. The forward PCET rate is nearly two orders of magnitude slower than measured for covalently linked Zn(II) porphyrin–acceptor dyads of comparable driving forces [46,47]. These results speak directly to the pronounced effect a proximal proton transfer network can have on an ET rate.

This influence of a proton network on ET rates is becoming more apparent as the structural details of biological systems are revealed. For instance, consider the GTB's treatment of the $^{\bullet}Y_Z$ radical of PS II [10]. The appropriate redox potentials needed for the evolution from energy migration to electron transfer to water oxidation in PS II

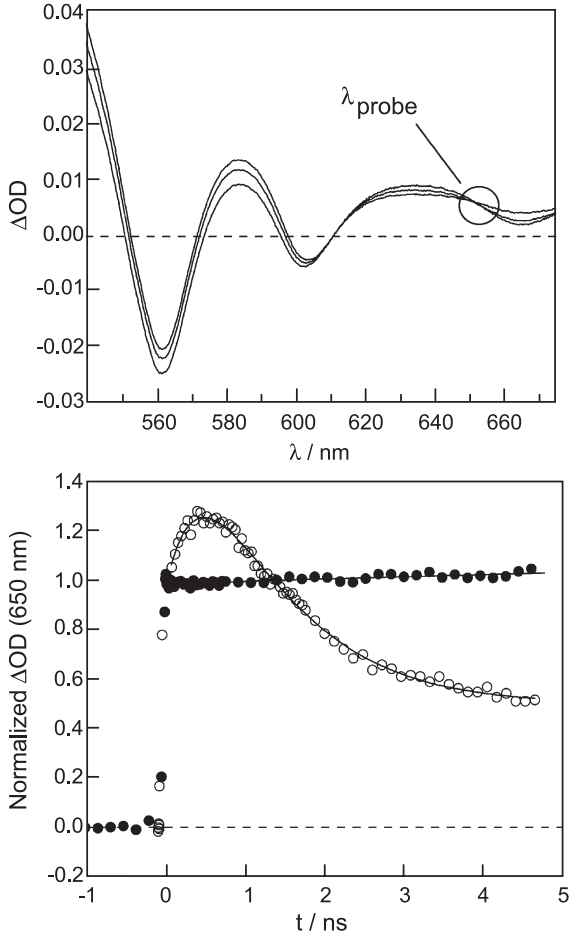

Fig. 5. (top) Transient spectra of **1** in THF collected 500 ps 1 ns and 2 ns after excitation. (bottom) Transient kinetics for porphyrin in absence of quencher (solid dots) and in the presence of quencher (open dots) (i.e., complex **1**) probed at the S_1-T_1 isosbestic point of the porphyrin. Both spectra and kinetics were collected using a 405-nm, 120-fs laser excitation pulse.

is controlled by D1-H190. In GTB's model, the proton from Y_Z either leaves simultaneously with the electron upon oxidation of the tyrosine or Y_Z is involved in a proton pre-equilibrium with its hydrogen-bonding partner, D1-H190. In either case, the proximal proton transfer network controls ET, a feature that we are able to isolate in D–[H^+]–A systems such as **1**.

The results of Fig. 5 are noteworthy because they are the first to provide kinetics from directly detected intermediates of a PCET reaction in a salt-bridge assembly. However, the timing of the proton transfer has not been achieved because the porphyrin shows only modest spectral shifts with the protonation state of the amidine functionality. Instead, we are only afforded optical signatures pertinent to the electron transfer component of the reaction. Steric clashing between the exo protons of the amidinium interface with the protons on the macrocycle causes the amidinium to rotate out of the macrocyclic plane; geometry optimizations for **1** show that the amidinium is canted by 34°. This canting electronically decouples the amidinium functionality from the porphyrin chromophore. Current efforts are underway to synthesize new amidinium porphyrins in which the steric clashing between salt-bridge interface and porphyrin macrocycle is relieved while maintaining conjugation between the two moieties.

3. The PCET pathway of ribonucleotide reductase (RNR)

PCET in biology is often synonymous with radical transport among amino acids. Accordingly, we have begun developing new biochemical and biophysical methods for investigating the mechanism of radical initiation and transport. RNR has been the focal point of these studies [48] because (i) the enzyme displays the consummate PCET pathway in biology by transferring an electron and proton over 35 Å across two subunits and (ii) modern biochemical techniques permit PCET in RNR to be examined at the same level of mechanistic rigor that we have achieved for D–[H^+]–A assemblies.

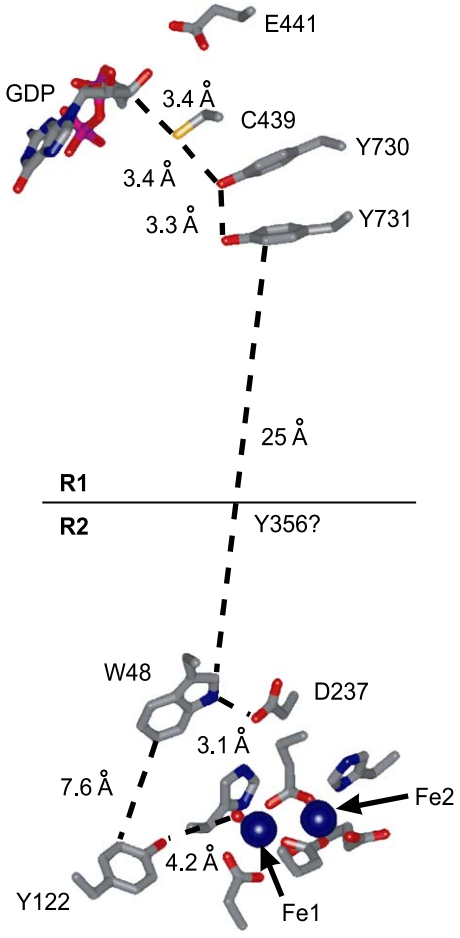

Fig. 6. Proposed PCET pathway in *E. coli* RNR based on a docking model of the R1 (α2) and R2 (β2) subunit structures [59] of *E. coli* RNR. PCET studies during the past period have focused on Y356 on the C-terminus of R2 (this residue is thermally labile and thus its position is not known) and Y731 and Y730, which are along the path to the active site cysteine C439.

RNRs catalyze the reduction of the four common ribonucleotides to their corresponding deoxyribonucleotides through a thiyl radical hydrogen abstraction mechanism [49–53]. RNRs have been divided into three classes based on the metallocofactor required for the radical initiation process [54–56]. All classes have an identical capacity of radical chain initiation, effectively propagating an H• radical from the metallocofactor site to a catalytic cysteine, whereupon it is transferred to the substrate during nucleotide reduction. [49,57,58]. Structures at atomic resolution of the *E. coli* R1 [59,60] and R2 [61] as well as the mouse [62], and yeast R2 [63] class I enzymes have been reported, though an active complex of R1 and R2 has yet to be crystallographically characterized.

The proposed 35-Å PCET pathway for the Class I enzymes shown in Fig. 6 has been constructed from the docking of crystal structures of the *E. coli* subunits [59,64]. The distances between Y122 and W48 on R2 and Y731 and C439 on R1 are known whereas the distance between W48 and Y731 is estimated to be 25 Å based on the docking model. Y356 (located on the C-terminus of R2) is an absolutely conserved residue [59,64] and is thought to be positioned between W48 and Y731 (this residue cannot be located because it is thermally labile in crystal structures). The hole migration from Y122•, generated at the binuclear iron center of the R2 subunit, to C439 and back, is believed to occur on each conversion of a nucleotide to a deoxynucleotide [65,66].

Extensive discussion has accompanied the construction of the PCET pathway shown in Fig. 6 [67–70]. The oxidizing power of a tyrosyl radical (+0.84 V vs. NHE) is insufficient for generating a thiyl radical from cysteine thiol (+1.33 V vs. NHE), and thus only oxidation of a deprotonated cysteine thiolate (+0.77 V vs. NHE) is favored, implicating a PCET mechanism [66]. Theoretical studies support this contention by showing proton and electron synchronization for H• to be highly favored over simple ET through R1 [71]. Experimentally, the PCET pathway has been studied to date most thoroughly by site-directed mutagenesis. Mutants of every residue in the putative pathway of Fig. 6 have been generated [67–70,72–75]. Whereas these studies have established that the mutant proteins are inactive, they have not shown the existence of amino acid radical intermediates along the proposed pathway or provided any further mechanistic details of the PCET process.

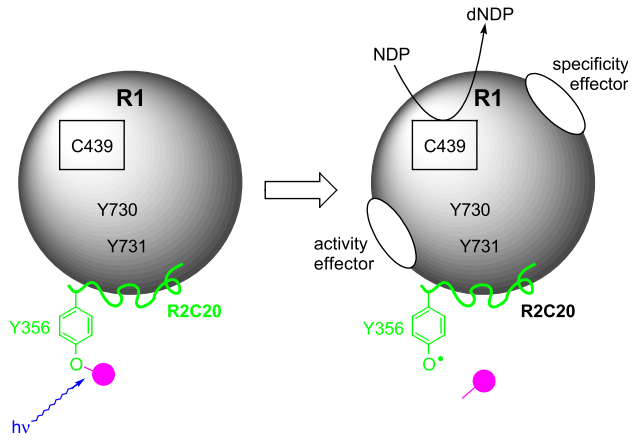

Fig. 7. The strategy being pursued for studying the Y731 → Y730 → C439 PCET pathway in R1 of RNR. NDP = nucleoside diphosphate substrate and dNDP = deoxy nucleoside-diphosphate product.

We have undertaken studies of the PCET pathway of Fig. 6 by isolating it to the individual R2 and R1 subunits. Our initial studies have tackled the putative Y356 → Y731 → Y730 transfer within the R1 subunit. The general strategy developed for these studies is depicted in Fig. 7. The 20-mer C-terminal peptide tail of the R2 subunit, containing both the critical Y356 as well as the R1 binding determinants [76], is the only part of the R2 subunit that has been retained. The objective during the initial stages of the work has been to synthesize the 20-mer peptide containing photo-triggers for tyrosyl radical generation. In this way, laser excitation of the modified peptide provides a method for generating Y356•, while bypassing hole generation at the metallocofactor. The approach allows us, in principle, to instantaneously "turn on" the PCET pathway in the R1 subunit in RNR.

The implementation of the approach shown in Fig. 7 demands the development of new photochemical methods for the laser decaging of amino acid radicals, with emphasis on tyrosine. We have developed one method for the generation of tyrosyl radical based on the photolysis chemistry of diaryl oxalate esters [77]. Both symmetric (**2**) and asymmetric (**3**, **4**) caged tyrosyl radicals were prepared on gram-scale. Photolysis of the oxalate-modified tyrosine results in the homolysis of the carbon-oxygen bond with the concomitant loss of two equivalents of carbon monoxide and the appearance of a tyrosyl and aryloxyl radical pair.

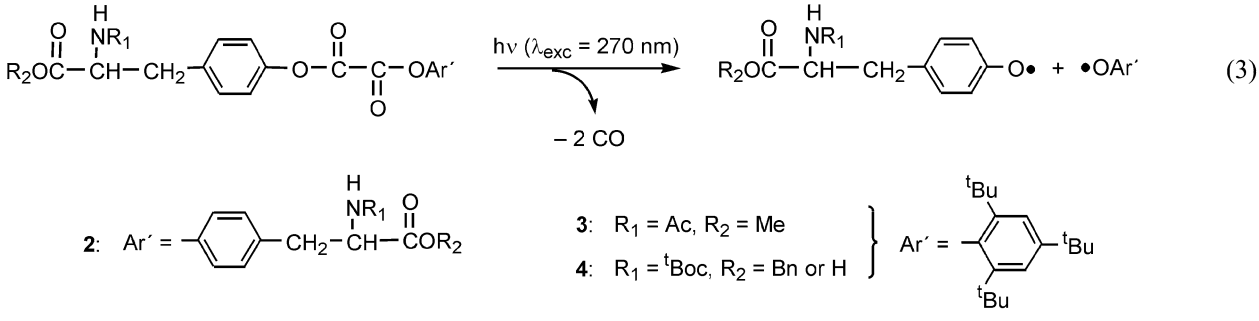

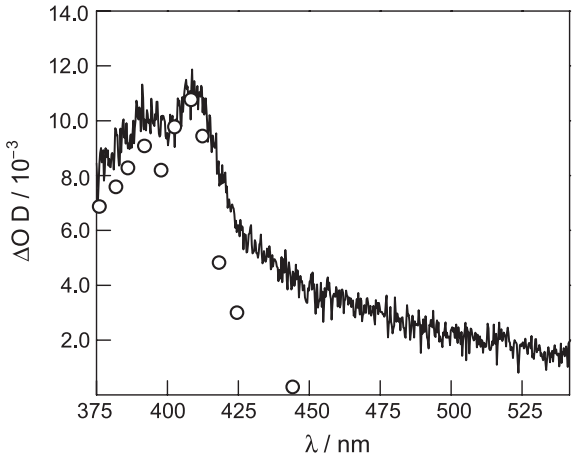

Fig. 8. Transient absorption spectrum of the tyrosyl radical formed from laser flash-photolysis of compound **2** overlaid on a spectrum of a tyrosyl radical (○) taken from Ref. [115]. The two spectra are normalized with respect to each other.

Time-resolved absorption spectroscopy of **2** reveals that the tyrosyl radical is produced within 50 ns after laser excitation (λ_{exc} = 270–300 nm) with a quantum yield of 10% (Fig. 8) [77]. Spin trapping by DMPO confirms the formation of Y·. Compound **3** undergoes a similar photo-induced decaging to deliver a tyrosyl radical and the sterically protected 2,4,6-tri-*tert*-butylphenoxyl radical on the same time scale. The hydrogenation of the benzyl ester moiety of **3** to yield free carboxylic acid delivers a functional group to couple these amino acid derivatives through the C-terminus. A wide variety of other N-terminal protecting groups, such as Fmoc or acetyl, are compatible with the deprotection and can be integrated into this class of compounds (**4**). Because the oxalate linkage does not persist under conditions required to cleave the peptide from the resin, the modified tyrosine is best introduced in solution phase synthesis, prompting us to abandon this line of inquiry. Nevertheless, this method should be useful to many in the biochemistry and enzymology communities who can tolerate a post solid-phase peptide synthetic step.

In light of the foregoing issues with oxalates, we have pursued a second strategy that relies on the photogeneration of tyrosyl radicals by electronically excited metal complexes. As Magnuson et al. [79] have shown, the flash-quench technique [78] permits the generation of a tyrosyl radical appended to a polypyridine ligand of a Ru(II) center. By developing alternative coupling strategies, we have appended $Ru^{II}(bpy)_3$ to the end of R2C20; the resulting modified peptide, $(bpy)_2$Ru(Mebpy)-R2C20, is stable to cleavage conditions in trifluoroacetic acid, thus allowing us to successfully employ solid phase techniques. The ruthenated peptide has been purified to homogeneity and fully characterized; a competition assay with R2 shows that the affinity of $(bpy)_2$Ru(Mebpy)$_3$-R2C20 for the R1 subunit of RNR is similar to that for the unmodified peptide AcR2C20 [80].

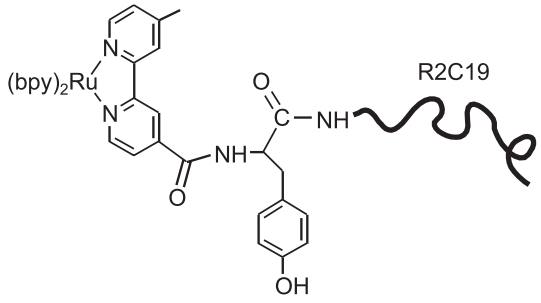

(bpy)$_2$Ru(Mebpy)–R2C20

Photolysis of $(bpy)_2$Ru(Mebpy)$_3$-R2C20 in the presence of a quencher such as $[Co(NH_3)_5Cl]^{2+}$ generates a tyrosyl radical at the essential Y356 position as follows,

$$(bpy)_2Ru^{II}(Mebpy) - Y - R2C19 + [Co^{III}(NH_3)_5Cl]^{2+} \xrightarrow{h\nu} (bpy)_2Ru^{III}(Mebpy) - Y - R2C19 + [Co^{II}(NH_3)_5Cl]^{+} \xrightarrow{ET} (bpy)_2Ru^{II}(Mebpy) - Y\cdot - R2C19 + [Co^{II}(H_2O)_6]^{2+} \quad (4)$$

This flash-quench reaction initiates hole transport into the R1 active site for turnover as diagrammed in Fig. 7. Under

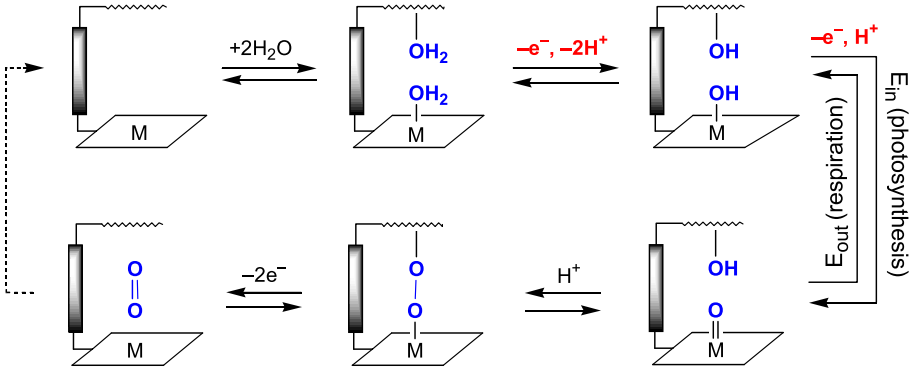

Fig. 9. A strategy for the PCET activation of oxygen and water at molecularly engineered active sites.

single turnover conditions, preliminary results are consistent with the light-mediated nucleotide reduction process catalyzed by the $(bpy)_2Ru(Mebpy)$-R2C20/R1 complex [80]. In the presence of light, radiolabelled product is detected by HPLC in the reaction mixture; in the absence of light, no radioactive product is detectable in the same reaction mixture. However, these results are complicated by the high radioactive background relative to the amount of product. The low activity results because the Ru(III) oxidant produced from the flash quench reaction of Eq. (4) has barely enough potential to oxidize tyrosine ($\sim$ 250 mV driving force). Indeed, Magnuson et al. [79] have shown that the tyrosine oxidation step in Eq. (4) proceeds with a unimolecular rate constant of only 5×10^4 s^{-1}. We will need to increase the yield of tyrosyl radical produced at Y356 in order to increase our signal-to-background ratio in this experiment. To accomplish this, we have turned our attention to increasing the oxidizing power of the photosensitizer appended to the terminus of R2C20. One approach is to replace the Ru(II) polypyridyl with a Re(I) polypyridyl. As Di Bilio et al. [81] have recently shown, the MLCT excited state of $Re(CO)_3(phen)(His)$ may be flash-quenched to produce a powerfully oxidizing Re(II) intermediate that is capable of generating tyrosyl and tryptophan radical species. In addition to metal-based oxidants, we are also pursuing a variety of organic methods to generate $Y356^{\cdot}$ by hydrogen atom abstraction, including natural and unnatural amino acids. The simple addition of an N-terminal tryptophan to R2C20 is sufficient to trigger Y356 oxidation upon irradiation at λ_{exc}>285 nm. Although this process occurs within the proteins absorption envelope, we have observed a significant amount of dCDP formation upon photolysis of Ac-W-R2C20 in the presence of R1 and allosteric effector [82]. As the 20-mer peptide alone has proven competent to mimic the conformational changes in R1 required for turnover, this approach promises to resolve many unanswered questions about the PCET pathway of RNR.

The foregoing studies target the PCET pathway in R1. PCET investigations within the R2 subunit are afforded by intein splicing methods [83–85]. For this protein semisynthesis approach, a modified peptide can be ligated to a truncated parent to furnish the mature protein with site-specific modifications. R2 is an excellent candidate for this type of semisynthesis since the residue of interest, Y356, is at the C-terminal tail of the enzyme. Indeed, R2 proteins with Y356 replaced by unnatural fluoro- [86] and nitrotyrosines [87] have recently been prepared by the splicing method. The technique is generally applicable for the placement of virtually any amino acid derivative at Y356 or anywhere within the C-terminus.

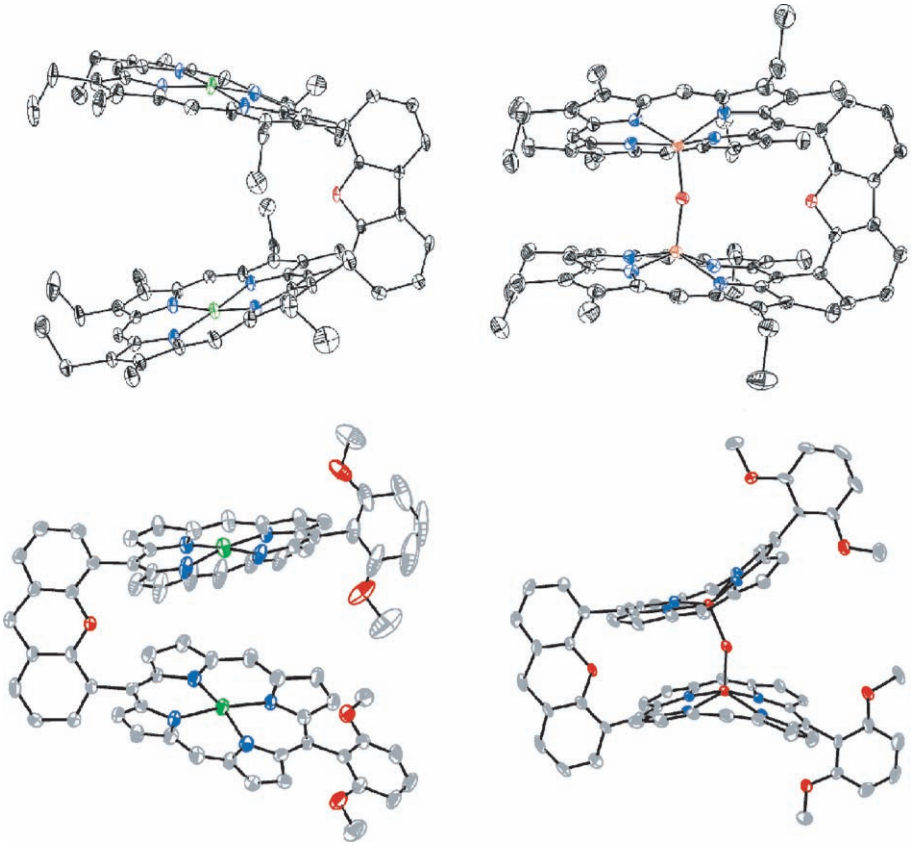

Fig. 10. The molecular structures of the Zn_2 (left) and the Fe_2 μ-oxo (right) bisporphyrins for the (a) DPX and (b) DPXM Pacman platforms.

We are currently expanding the scope of the semisynthetic technique to include photoactive tyrosine derivatives. In this way, radical transport within R2 may be investigated akin to the approaches being developed for PCET studies in R1.

4. O–O bond catalysis by PCET

The mechanistic insights acquired from PCET model systems provide a roadmap to develop new platforms for catalytically activating oxygen and water by PCET. The D-[H^+]-A systems of Section 2, combining acid–base and redox functionalities on a single molecular platform, contain the rudimentary elements needed for PCET activation. However, these functionalities are not ideally presented for the examination of PCET as it pertains to small-molecule activation chemistry. Acid–base and redox sites are side-to-side, thus orienting the PCET functionalities orthogonal to catalytic bond-making and bond-breaking processes occurring at the metal center of the porphyrin. In order to direct proton transfer along the coordination axis of small-molecule activation, we sought to create constructs where proton and electron delivery were confined to a face-to-face arrangement:

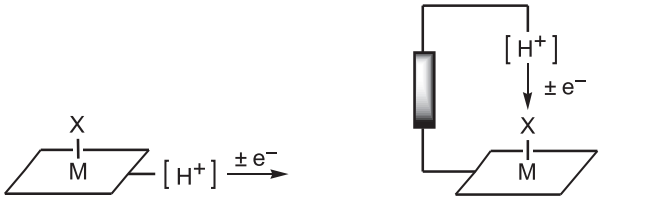

side-to-side PCET networks face-to-face PCET networks

Such face-to-face PCET networks allow key elements of oxygen–oxygen bond breaking and bond-making activation to be investigated. Fig. 9 schematically depicts the pathway for water activation, and the microscopic reverse, oxygen activation, using a redox platform with a cofacially oriented proton transfer network. Akin to GTB's scheme of Fig. 1, conversion between peroxo and metal oxo-hydroxo intermediates emerges as a mechanistic theme for oxygen and water activation.

Our first generation approach to elaborating Fig. 9 has utilized porphyrins to support the nascent oxo and neighboring hydroxo. This starting point of bisporphyrins cofacially presented by a single rigid pillar builds on the pioneering work of Collman and GTB's colleague and friend, C.K. Chang. In their designs, the cofacial bisporphyrins, designated "Pacman" porphyrins, were juxtaposed by anthracene (DPA) and biphenylene (DPB) pillars [88–91]. The architecture confines two porphyrins in a face-to-face geometry with little lateral and vertical displacement; the pocket sizes of the DPA and DPB cofacial porphyrins differed by ca. 1 Å. With regard to Fig. 9, these Pacman porphyrins containing late transition metals (e.g., Co) have been quite prominent as electrocatalysts for the reduction of oxygen [91]. However, the cofacial motif poses a problem when porphyrins contain earlier transition metals such as Fe and Mn, which are needed for bond-breaking *and* bond-making chemistry of oxygen. The high thermodynamic driving force for M_2 μ-oxo formation,

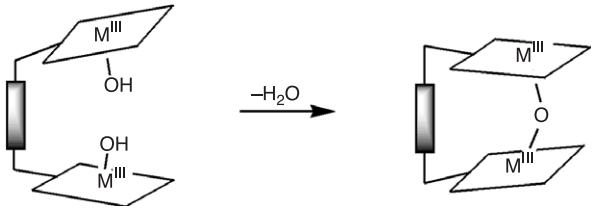

(5)

is a significant impediment to the chemistry of Fig. 9. We therefore sought to engineer new cofacial bisporphyrins displaying an expanded pocket with the goal of hindering μ-oxo formation. Toward this end, we have recently demonstrated that xanthene and dibenzofuran spacers can organize two redox cofactors along the desired face-to-face reaction coordinate [92,93]. In these diporphyrin xanthene (DPX) and diporphyrin dibenzofuran (DPD) cofacial constructs, neighboring porphyrins display an extensive range of vertical pocket size dimensions and flexibilities with minimal lateral displacements between macrocyclic subunits.

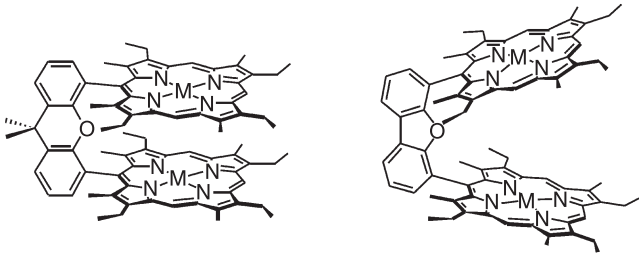

DPX DPD

By employing appropriate substituents along the periphery of the macrocyclic superstructure, it is possible to tune the pocket sizes of the Pacman motif in increments of 0.5 Å over a series of metal-metal distances ranging from 3.5 Å to over 8.5 Å [94–96]. Similar to DPA and DPB Pacman porphyrins, the dicobalt(II) complexes of both DPX and DPD are effective electrocatalysts for the direct four-electron, four-proton reduction of oxygen to water over the more common two-electron, two-proton reduction to hydrogen peroxide [97]. However, comparative structural [98] and steady-state [99] and time-resolved reactivity [100] studies of the early transition metal porphyrins reveal that neither

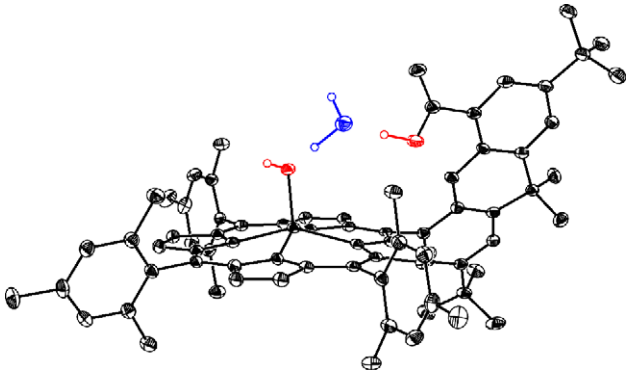

Fig. 11. The molecular structure of the heme water channel model, $Fe^{III}(OH)(HPX\text{-}CO_2H)$.

large vertical pocket sizes nor substituents around the porphyrin periphery impede μ-oxo formation. As shown in Fig. 10, the Fe_2 μ-oxo core may form by either opening or closing the binding pocket of the DPD system by a vertical distance of over 4 Å (Fig. 10a) or by distorting of the macrocyclic ring of the sterically encumbered DPXM system (methoxyaryl groups at meso positions *trans* to the DPX spacer) (Fig. 10b).

In addition to μ-oxo formation, the inability to control proton transport to and from the redox platform of Pacman porphyrins presents obvious challenges to investigations based on Fig. 9. Both drawbacks are overcome when one porphyrin redox subunit is replaced with a proton donor. We have shown that a xanthene anchor may be used to "hang" a hydrogen-bond functionality over a redox-active metalloporphyrin platform [101]. These resulting hybrid proton/redox shuttle platforms, which have been designated Hangman porphyrins (HPX), are simplified constructs of biomolecules with engineered distal sites [102–104]. They capture control of both the proton and electron transfer but with reduced complexity since secondary and tertiary protein structures are not required to impose a proton network among structured water or protonated amino acid side chains.

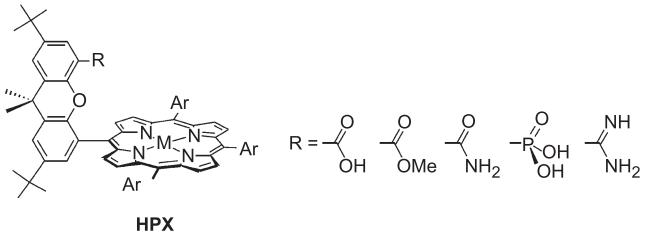

HPX

The Hangman construct allows for precise control over the functional nature of the hydrogen-bonding group in terms of proton-donating ability and arrangement in relation to the metalloporphyrin redox site. The carboxylic acid derivative has led to an especially fruitful study of PCET. The structure of the iron complex, shown in Fig. 11 [105], represents the first structurally characterized monomeric iron(III) hydroxide porphyrin. Even more striking is the water molecule bound between the xanthene carboxylic acid and the hydroxide ligand. This is the first model of a redox-active site displaying a structurally well-defined proton transfer network. This unique structural motif captures the essence of the monooxygenases in which structured water is proposed to finely tune heme electronic structure and redox potential, as well as providing a possible proton-relay during multielectron catalysis. Notably, spectroscopic data for $Fe^{III}OH(HPX)$ indicate that the water molecule remains bound in solution as well as in the solid state, and that this binding is chemically reversible. The measured binding energy of water is 5.8 kcal/mol. The HPX platform thus provides a geometrically matched microcavity for examination of PCET-mediated O—O bond activation and formation by juxtaposing two oxygen atoms between proton and electron transfer sites.

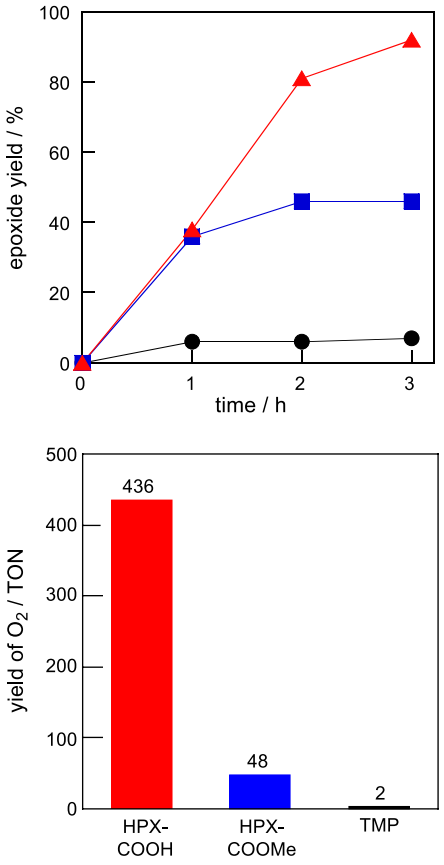

Fig. 12. (a) Time-course plot for the epoxidation of *cis*-cyclooctene with hydrogen peroxide catalyzed by Mn(HPX-COOH) (▲), Mn(HPX-COOMe) (■) and MnCl(TMP) (●). (b) Turnover numbers (TON) for oxygen release from H_2O_2 dismutation catalyzed by Fe^{III}(HPX-COOH), Fe^{III}(HPX-COOMe) and $Fe^{III}Cl$(TMP). For both reactions, the addition of 1 equiv benzoic acid to the TMP control shows no detectable enhancement in catalytic reactivity.

The active site is unique because it displays two different types of reactivities. Catalase-like oxygen evolution is observed for the iron complex and cytochrome P450-type epoxidation is observed for the manganese complex [106]:

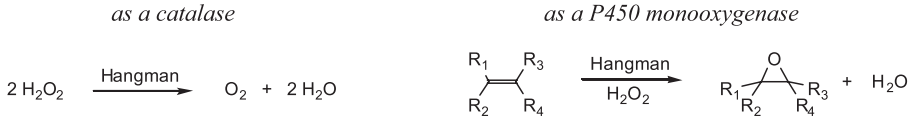

(6)

We have evaluated this O—O bond catalysis for a set of HPX and HPD compounds with varying hydrogen-bonding and proton-transfer abilities [107]. From a roster of eight different systems (pK_as ranging from 1.8 to 25), we have found that the most effective catalysts for effecting reactions in Eq. (6) possess hanging groups with $pK_a < 5$ (R = COOH and $P(O)(OH)_2$). Control experiments using a simple redox-only porphyrin analog with similar steric and electronic properties (TMP = 5,10,15,20-tetramesitylporphyrin) and a hanging group with no acid–base functionality (i.e., ester) reveal that a single well-positioned proton transfer site engenders remarkable activity (see Fig. 12). The proposed catalytic pathway for the O—O reactivity of the most active xanthene-bridged HPX-COOH platform is shown in Fig. 13. Reaction of H_2O_2 with the porphyrin in the presence of an axial ligand results in a putative metal hydroperoxide complex. A crucial proton transfer to the bound HO_2^- species promotes heterolytic O—O bond cleavage to produce the active oxoiron(IV) porphyrin cation radical or an oxomanganese(V) catalyst. Independent spectroscopic measurements establish that the HPX scaffold supports such high-valent oxo compounds [106]. As implied by the cycle in Fig. 13, the HPX-COOH system can stabilize the binding of oxidant by hydrogen bonding, while the carboxylic acid group provides an intramolecular shuttle that delivers proton equivalents for oxidation chemistry. We believe that the confluence of these two factors is responsible for the exceptional catalytic activity of the Hangman porphyrins.

The Hangman strategy has significant implications from the perspectives of both biological enzymes and catalyst

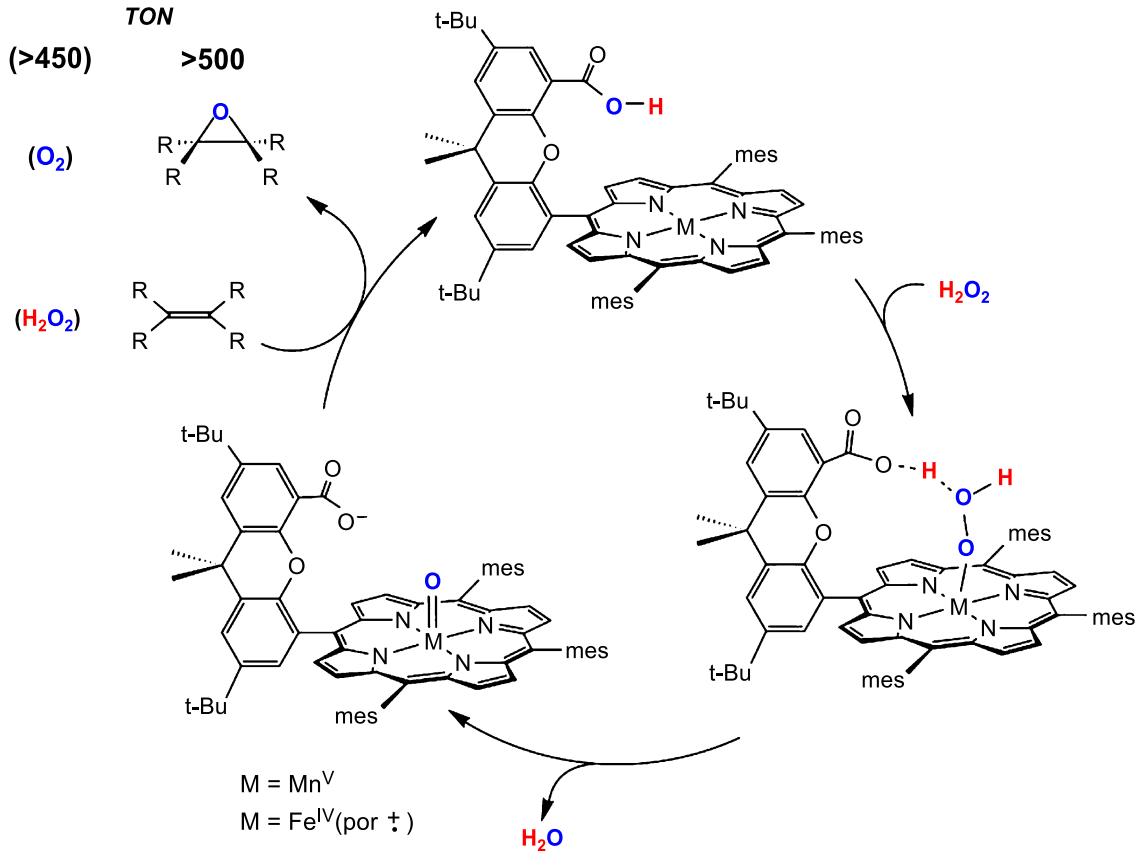

Fig. 13. Proposed cycle for the O—O activation by PCET catalysis of the Hangman platform, Fe^{III}(HPX-COOH). For epoxidations, the Mn^{V}=O is the active catalyst.

design. First, the ability to achieve efficient catalase and epoxidation activity using a single metalloporphyrin-based scaffold is evocative of natural heme-dependent proteins that employ a conserved protoporphyrin IX cofactor to effect a myriad of chemical reactivities. The crucial proton transfer needed for the transformation of iron peroxy to the catalytically active compound type I in the active sites of a variety of heme enzymes, including prostaglandin endoperoxide synthase-1 [108], peroxidases [109–111], and cytochrome P450 [112], is faithfully captured in the Hangman active site. In terms of synthetic catalyst design, the Hangman strategy demonstrates that the addition of proton control to a redox platform can enhance its catalytic performance. The importance of hydrogen bonding for controlling oxygen activation has recently been demonstrated by the *stoichiometric* reactions of oxygen and water within tripodal non-heme cavities [113,114]. The Hangman approach is distinguished by its ability to use a hydrogen-bond network to actively deliver protons to drive *catalytic* oxygen activation processes. We anticipate that further development of hybrid architectures containing both acid–base and redox functionalities will lead to new advances in catalysis. Finally, the divergent oxidation reactivity displayed by the Hangman systems finds its origins in GTB's unified model for oxygen/water activation (Fig. 1). With its structurally well-defined proton transfer network, juxtaposed to the redox site for O—O bond activation, the HPX scaffold provides a testbed for investigating GTB's contention that the peroxo⇌hydroxo/oxo interconversion is paramount to oxygen–oxygen bond-making and bond-breaking reactions.

5. Concluding remarks

GTB's introduction to the PCET problem began with his interest in the radical signatures of PS II. By following the chemistry of the tyrosyl radical into the OEC active site, he made the critical connection between PCET and water activation. His parallel interest in cytochrome *c* oxidase subsequently led to him to propose a unified PCET mechanism for oxygen/water activation. During his scientific journey, GTB uncovered PCET as an essential element in biology—as a primary mechanism of charge transport, at the underpinning of amino acid radical initiation and transport, and at the crux of water and oxygen activation at the active sites of PS II and cytochrome *c* oxidase. These same three elements form the basis for our studies of PCET and, in this way, GTB's spirit lives on in our science. My students and I find this to be a happy consequence of our work.

Acknowledgements

We thank all of our coworkers who have worked on this project over the years and Professor JoAnne Stubbe, who is a wonderful colleague and collaborator on PCET studies of RNR. The National Institutes of Health (GM47274) supported the research presented in this review. C.J.C. and M.C.Y.C. both kindly thank the National Science Foundation and the MIT/Merck Foundation for predoctoral fellowships. N.H.D. thanks the National Institutes of Health for a Postdoctoral Fellowship.

References

[1] J. Stubbe, W.A. van der Donk, Protein radicals in enzyme catalysis, Chem. Rev. 98 (1998) 705–762.
[2] G.T. Babcock, K. Sauer, Electron paramagnetic resonance signal II in spinach chloroplasts: I. Kinetic analysis for untreated chloroplasts, Biochim. Biophys. Acta 325 (1973) 483–503.
[3] G.T. Babcock, K. Sauer, Electron paramagnetic resonance signal II in spinach chloroplasts: II. Alternative spectral forms and inhibitor effects on kinetics of signal II in flashing light, Biochim. Biophys. Acta 325 (1973) 504–519.
[4] G.T. Babcock, K. Sauer, A rapid, light-induced transient in electron paramagnetic resonance signal II activated upon inhibition of photosynthetic oxygen evolution, Biochim. Biophys. Acta 376 (1973) 315–328.
[5] G.T. Babcock, K. Sauer, The rapid component of electron paramagnetic resonance signal II: a candidate for the physiological donor to photosystem II in spinach chloroplasts, Biochim. Biophys. Acta 376 (1975) 329–344.
[6] R.E. Blankenship, G.T. Babcock, J.T. Warden, K. Sauer, Observation of a new EPR transient in chloroplasts that may reflect the electron donor to photosystem II at room temperature, FEBS Lett. 51 (1975) 287–293.
[7] R.E. Blankenship, G.T. Babcock, K. Sauer, Kinetic study of oxygen evolution parameters in triswashed, reactivated chloroplasts, Biochim. Biophys. Acta 387 (1975) 165–175.
[8] B.A. Barry, G.T. Babcock, Tyrosine radicals are involved in the photosynthetic oxygen-evolving system, Proc. Natl. Acad. Sci. U. S. A. 84 (1987) 7099–7103.
[9] G.T. Babcock, B.A. Barry, R.J. Debus, C.W. Hoganson, M. Atamian, L. McIntosh, I. Sithole, C.F. Yocum, Water oxidation in photosystem II: from radical chemistry to multielectron chemistry, Biochemistry 28 (1989) 9557–9565.
[10] An excellent summary of the role of Y_Z in the chemistry of PSII can be found in C. Tommos, G.T. Babcock, Proton and hydrogen currents in photosynthetic water oxidation, Biochim. Biophys. Acta 1458 (2000) 199–219.
[11] K.L. Westphal, N. Lydakis-Simantiris, R.I. Cukier, G.T. Babcock, Effects of Sr^{2+}-substitution on the reduction rates of $\cdot Y_Z$ in PSII membranes—evidence for concerted hydrogen-atom transfer in oxygen evolution, Biochemistry 39 (2000) 16220–16229.
[12] K.L. Westphal, C. Tommos, R.I. Cukier, G.T. Babcock, Concerted hydrogen-atom abstraction in photosynthetic water oxidation, Curr. Opin. Plant Biol. 3 (2000) 236–242.
[13] M. Sjödin, S. Styring, B. Åkermark, L. Sun, L. Hammarström, Proton-coupled electron transfer from tyrosine in a tyrosine-ruthenium-tris-bipyridine complex: comparison with tyrosine Z oxidation in photosystem II, J. Am. Chem. Soc. 122 (2000) 3932–3936.
[14] C. Tommos, G.T. Babcock, Oxygen production in nature: a light-driven metalloradical enzyme process, Acc. Chem. Res. 31 (1998) 18–25.
[15] W. Junge, M. Haumann, R. Ahlbrink, A. Mulkidjanian, J. Clausen, Electrostatics and proton transfer in photosynthetic water oxidation, Philos. Trans. R. Soc. Lond., B 357 (2002) 1407–1418.
[16] C. Tommos, Electron, proton and hydrogen-atom transfers in photosynthetic water oxidation, Philos. Trans. R. Soc. Lond., B 357 (2002) 1383–1394.

[17] J.M. Peloquin, K.A. Campbell, D.W. Randall, M.A. Evanchik, V.L. Pecoraro, W.H. Armstrong, R.D. Britt, ^{55}Mn ENDOR of the S_2-state multiline EPR signal of photosystem II: implications on the structure of the tetranuclear Mn cluster, J. Am. Chem. Soc. 122 (2000) 10926–10942.
[18] C.W. Hoganson, M.A. Pressler, D.A. Proshlyakov, G.T. Babcock, From water to oxygen and back again: mechanistic similarities in the enzymatic redox conversions between water and dioxygen, Biochim. Biophys. Acta 1365 (1998) 170–174.
[19] V.K. Yachandra, K. Sauer, M.P. Klein, Manganese cluster in photosynthesis: where plants oxidize water to dioxygen, Chem. Rev. 96 (1996) 2927–2950.
[20] A. Zouni, H.T. Witt, J. Kern, P. Fromme, N. Krauss, W. Saenger, P. Orth, Crystal structure of photosystem II from *Synechococcus elongatus* at 3.8 Å resolution, Nature 409 (2001) 739–743.
[21] R.A. Marcus, N. Sutin, Electron transfers in chemistry and biology, Biochim. Biophys. Acta 811 (1985) 265–322.
[22] R.A. Marcus, Electron-transfer reactions in chemistry: theory and experiment, Angew. Chem., Int. Ed. Engl. 32 (1993) 1111–1121.
[23] C.J. Chang, J.D.K. Brown, M.C.Y. Chang, E.A. Baker, D.G. Nocera, Electron transfer in hydrogen-bonded donor–acceptor supramolecules, in: V. Balzani (Ed.), Electron Transfer in Chemistry, vol. 3.2.4. Wiley, Weinheim, Germany, 2001, pp. 409–461.
[24] R.I. Cukier, D.G. Nocera, Proton-coupled electron transfer, Annu. Rev. Phys. Chem. 49 (1998) 337–369.
[25] C. Turró, C.K. Chang, G.E. Leroi, R.I. Cukier, D.G. Nocera, Photoinduced electron transfer mediated by a hydrogen-bonded interface, J. Am. Chem. Soc. 114 (1992) 4013–4015.
[26] R.I. Cukier, S. Daniels, E. Vinson, R.J. Cave, Are hydrogen bonds unique among weak interactions in their ability to mediate electronic coupling? J. Phys. Chem., A 106 (2002) 11240–11247.
[27] X.G. Zhao, R.I. Cukier, Molecular dynamics and quantum chemistry study of a proton-coupled electron transfer reaction, J. Phys. Chem. 99 (1995) 945–954.
[28] R.I. Cukier, Mechanism for proton-coupled electron-transfer reactions, J. Phys. Chem. 98 (1994) 2377–2381.
[29] J.L. Sessler, B. Wang, S.L. Springs, C.T. Brown, Electron- and energy-transfer reactions in noncovalently linked supramolecular model systems, in: Y. Murakami (Ed.), Comprehensive Supramolecular Chemistry, vol. 4. Pergamon Press, Oxford, 1996, pp. 311–336.
[30] M.D. Ward, Photoinduced electron and energy transfer in non-covalently bonded supramolecular assemblies, Chem. Soc. Rev. 26 (1997) 365–376.
[31] V.Y. Shafirovich, S.H. Courtney, N. Ya, N.E. Geacintov, Proton-coupled photoinduced electron transfer, deuterium isotope effects, and fluorescence quenching in noncovalent benzo[α]pyrenetetraol-nucleoside complexes in aqueous solutions, J. Am. Chem. Soc. 117 (1995) 4920–4929.
[32] T.H. Ghaddar, E.W. Castner, S.S. Isied, Molecular recognition and electron transfer across a hydrogen bonding interface, J. Am. Chem. Soc. 122 (2000) 1233–1234.
[33] J.A. Roberts, J.P. Kirby, D.G. Nocera, Photoinduced electron transfer within a donor–acceptor pair juxtaposed by a salt bridge, J. Am. Chem. Soc. 117 (1995) 8051–8052.
[34] Y. Deng, J.A. Roberts, S.M. Peng, C.K. Chang, D.G. Nocera, The amidinium-carboxylate salt bridge as a proton-coupled interface to electron transfer pathways, Angew. Chem., Int. Ed. Engl. 36 (1997) 2124–2127.
[35] J.A. Roberts, J.P. Kirby, S.T. Wall, D.G. Nocera, Electron transfer within ruthenium(II) polypyridyl-(salt-bridge)-dimethylaniline acceptor-donor complexes, Inorg. Chim. Acta 263 (1997) 395–405.
[36] J.P. Kirby, N.A. van Dantzig, C.K. Chang, D.G. Nocera, Formation of porphyrin donor–acceptor complexes via an amidinium-carboxylate salt bridge, Tetrahedron Lett. 36 (1995) 3477–3480.
[37] J.P. Kirby, J.A. Roberts, D.G. Nocera, Significant effect of salt bridges on electron transfer, J. Am. Chem. Soc. 119 (1997) 9230–9236.
[38] S. Hammes-Schiffer, Proton-coupled electron transfer, in: V. Balzani (Ed.), Electron Transfer in Chemistry, vol. 1.1.5. Wiley, Weinheim, Germany, 2001, pp. 189–237.
[39] R.I. Cukier, A theory that connects proton-coupled electron-transfer and hydrogen-atom transfer reactions, J. Phys. Chem., B 106 (2002) 1746–1757.
[40] R.I. Cukier, Proton-coupled electron transfer reactions: evaluation of rate constants, J. Phys. Chem. 100 (1996) 15428–15443.
[41] A. Soudackov, S. Hammes-Schiffer, Derivation of rate expressions for nonadiabatic proton-coupled electron transfer reactions in solution, J. Chem. Phys. 113 (2000) 2385–2396.
[42] C.Y. Yeh, S.E. Miller, S.D. Carpenter, D.G. Nocera, Structurally homologous β- and meso-amidinium porphyrins, Inorg. Chem. 40 (2001) 3643–3646.
[43] M. Ohkohchi, A. Takahashi, N. Mataga, T. Okada, A. Osuka, H. Yamada, K. Maruyama, Direct observation of a consecutive 2-step electron-transfer in some zinc porphyrin pyromellitimide quinone triads which undergo the same mode of electron transfers as in the bacterial photosynthetic reaction-center, J. Am. Chem. Soc. 115 (1993) 12137–12143.
[44] A.S. Lukas, M.R. Wasielewski, Approaches to an optically controlled molecular switch, in: V. Balzani (Ed.), Electron Transfer in Chemistry, vol. 5.1.2. Wiley, Weinheim, Germany, 2001, pp. 48–96.
[45] N.H. Damrauer, J. Hodgkiss, J. Rosenthal, D.G. Nocera, Observation of proton-coupled electron transfer by transient absorption spectroscopy in hydrogen-bonded, supramolecular porphyrin donor–acceptor assemblies, submitted for publication.
[46] M.R. Wasielewski, M.P. Niemczyk, W.A. Svec, E.B. Pewitt, Dependence of rate constants for photoinduced charge separation and dark charge recombination on the free energy of reaction in restricted-distance porphyrin-quinone molecules, J. Am. Chem. Soc. 107 (1985) 1080–1082.
[47] A. Osuka, R. Yoneshima, H. Shiratori, T. Okada, S. Taniguchi, N. Mataga, Electron transfer in a hydrogen-bonded assembly consisting of porphyrin-diimide, Chem. Commun. (1998) 1567–1568.
[48] J. Stubbe, D.G. Nocera, C.S. Yee, M.C.Y. Chang, Radical initiation in the class I ribonucleotide reductase: long range proton coupled electron transfer? Chem. Rev. 103 (2003) 2167–2201.
[49] S. Licht, G.J. Gerfen, J. Stubbe, Thiyl radicals in ribonucleotide reductases, Science 271 (1996) 477–481.
[50] J. Stubbe, Ribonucleotide reductases: amazing and confusing, J. Biol. Chem. 265 (1990) 5329–5332.
[51] L. Thelander, P. Reichard, Reduction of ribonucleotides, Annu. Rev. Biochem. 48 (1979) 133–158.
[52] A. Jordan, P. Reichard, Ribonucleotide reductases, Annu. Rev. Biochem. 67 (1998) 71–98.
[53] J. Stubbe, J. Ge, C.S. Yee, The evolution of ribonucleotide reduction revisited, Trends Biochem. Sci. 26 (2001) 93–99.
[54] S. Licht, J. Stubbe, Mechanistic investigations of ribonucleotide reductases, in: S.D. Barton, K. Nakanishi, O. Meth-Cohn, D.C. Poulter (Eds.), Comprehensive Natural Products Chemistry, vol. 5. Elsevier, New York, 1999, pp. 163–203.
[55] H. Eklund, M. Fontecave, Glycyl radical enzymes: a conservative structural basis for radicals, Structure Fold. Des. 7 (1999) R257–R262.
[56] H. Eklund, U. Uhlin, M. Farnegardh, D.T. Logan, P. Nordlund, Structure and function of the radical enzyme ribonucleotide reductase, Prog. Biophys. Mol. Biol. 77 (2001) 177–268.
[57] G.J. Gerfen, W.A. van der Donk, G. Yu, J.R. McCarthy, E.T. Jarvi, D.P. Matthews, C. Farrar, R.G. Griffin, J. Stubbe, Characterization of a substrate-derived radical detected during the inactivation of ribonucleotide reductase from *Escherichia coli* by 2′-fluoromethylene-2′-deoxycytidine 5′-diphospate, J. Am. Chem. Soc. 120 (1998) 3823–3835.

[58] D.J. Silva, J. Stubbe, V. Samano, M.J. Robins, Gemcitabine 5′ -triphosphate is a stoichiometric mechanism-based tnhibitor of *Lactobacillus leichmannii* ribonucleoside triphosphate reductase: evidence for thiyl radical-mediated nucleotide radical formation, Biochemistry 37 (1998) 5528–5535.
[59] U. Uhlin, H. Eklund, Structure of ribonucleotide reductase protein R1, Nature 370 (1994) 533–539.
[60] U. Uhlin, H. Eklund, The ten-stranded beta/alpha barrel in ribonucleotide reductase protein R1, J. Mol. Biol. 262 (1996) 358–369.
[61] P. Nordlund, B.M. Sjöberg, H. Eklund, Three-dimensional structure of the free radical protein of ribonucleotide reductase, Nature 345 (1990) 593–598.
[62] B.B.Nielsen,B.Kauppi,M.Thelander,L.Thelander,I.K.Larsen,Eklund, Eklund, H. Eklund, Crystallization and crystallographic investigations of the small-subunit of mouse ribonucleotide reductase crystallization and crystallographic investigations of the small-subunit of mouse ribonucleotide reductase, FEBS Lett. 373 (1995) 310–312.
[63] W.C. Voegtli, J. Ge, D.L. Perlstein, J. Stubbe, A.C. Rosenzweig, Structure of the yeast ribonucleotide reductase Y2Y4 heterodimer, Proc. Natl. Acad. Sci. U. S. A. 98 (2001) 10073–10078.
[64] B.M. Sjöberg, The ribonucleotide reductase jigsaw puzzle — a large piece falls into place, Structure 2 (1994) 793–796.
[65] J. Ge, G. Yu, M.A. Ator, J. Stubbe, Pre-steady state and steady state kinetic analysis of *E. coli* class I ribonucleotide reductase, Biochemistry 42 (2003) 10071–10083.
[66] J. Stubbe, P. Riggs-Gelasco, Harnessing free radicals: formation and function of the tyrosyl radical in ribonucleotide reductase, Trends Biochem. Sci. 23 (1998) 438–443.
[67] I. Climent, B.M. Sjöberg, C.Y. Huang, Site-directed mutagenesis and deletion of the carboxyl terminus of *Escherichia coli* ribonucleotide reductase protein R2. Effects on catalytic activity and subunit interaction, Biochemistry 31 (1992) 4801–4807.
[68] M. Sahlin, G. Lassmann, S. Pötsch, B.M. Sjöberg, A. Gräslund, Transient free radicals in iron/oxygen reconstitution of mutant protein R2 Y122F, J. Biol. Chem. 270 (1995) 12361–12372.
[69] B. Katterle, M. Sahlin, P.P. Schmidt, S. Pötsch, D.T. Logan, A. Gräslund, B.M. Sjöberg, Kinetics of transient radicals in *Escherichia coli* ribonucleotide reductase, J. Biol. Chem. 272 (1997) 10414–10421.
[70] M. Ekberg, P. Birgander, B.M. Sjöberg, In vivo assay for low-activity mutant forms of *E. coli* ribonucleotide reductase, J. Bacteriol. 185 (2003) 1167–1173.
[71] P.E.M. Siegbahn, L. Eriksson, F. Himo, M. Pavolv, Hydrogen atom transfer in ribonucleotide reductase, J. Phys. Chem., B 102 (1998) 10622–10629.
[72] M. Ekberg, S. Pötsch, E. Sandin, M. Thunnissen, P. Nordlund, M. Sahlin, B.M. Sjöberg, Preserved catalytic activity in an engineered ribonucleotide reductase R2 protein with a nonphysiological radical transfer pathway, J. Biol. Chem. 273 (1998) 21003–21008.
[73] M. Ekberg, M. Sahlin, M. Eriksson, B.M. Sjöberg, Two conserved tyrosine residues in protein R1 participate in an intermolecular electron transfer in ribonucleotide reductase, J. Biol. Chem. 271 (1996) 20655–20659.
[74] U. Rova, K. Goodtzova, R. Ingemarson, G. Behravan, A. Gräslund, L. Thelander, Evidence by site-directed mutagenesis supports long-range electron-transfer in mouse ribonucleotide reductase, Biochemistry 34 (1995) 4267–4275.
[75] U. Rova, A. Adrait, S. Pötsch, A. Gräslund, L. Thelander, Evidence by mutagenesis that Tyr370 of the mouse ribonucleotide reductase R2 protein is the connecting link in the intersubunit radical transfer pathway, J. Biol. Chem. 274 (1999) 23746–23751.
[76] I. Climent, B.M. Sjöberg, C.Y. Huang, Carboxyl-terminal peptides as probes for *E. coli* ribonucleotide reductase subunit interaction — kinetic analysis of inhibition studies, Biochemistry 30 (1991) 5164–5171.
[77] M.C.Y. Chang, S.E. Miller, S.D. Carpenter, J. Stubbe, D.G. Nocera, Nanosecond generation of tyrosyl radicals via laser-initiated decaging of oxalate-modified amino acids, J. Org. Chem. 67 (2002) 6820–6822.
[78] M.J. Bjerrum, D.R. Casimiro, I.J. Chang, A.J. Di Bilio, H.B. Gray, M.G. Hill, R. Langen, G.A. Mines, L.K. Skov, Electron-transfer in ruthenium-modified proteins, J. Bioenerg. Biomembranes 27 (1995) 295–302.
[79] A. Magnuson, H. Berglund, P. Korall, L. Hammarström, B. Åkermark, S. Styring, L.C. Sun, Mimicking electron transfer reactions in photosystem II: synthesis and photochemical characterization of a ruthenium(II) tris(bipyridyl) complex with covalently linked tyrosine, J. Am. Chem. Soc. 119 (1997) 10720–10725.
[80] M.C.Y. Chang, Ph.D. Thesis, MIT (2004).
[81] A.J. Di Bilio, B.R. Crane, W.A. Wehbi, C.N. Kiser, M.M. Abu-Omar, R.M. Carlos, J.H. Richards, J.R. Winkler, H.B. Gray, Properties of photogenerated tryptophan and tyrosyl radicals in structurally characterized proteins containing rhenium(I) tricarbonyl diimines, J. Am. Chem. Soc. 123 (2001) 3181–3182.
[82] M.C.Y. Chang, C.S. Yee, J. Stubbe, D.G. Nocera, Turning on ribonucleotide reductase by light-initiated amino acid radical generation, submitted for publication.
[83] R.M. Hofmann, T.W. Muir, Recent advances in the application of expressed protein ligation to protein engineering, Curr. Opin. Biotechnol. 13 (2002) 297–303.
[84] T.W. Muir, D. Sondhi, P.A. Cole, Expressed protein ligation: a general method for protein engineering, Proc. Natl. Acad. Sci. U. S. A. 95 (1998) 6705–6710.
[85] K. Severinov, T.W. Muir, Expressed protein ligation, a novel method for studying protein–protein interactions in transcription, J. Biol. Chem. 273 (1998) 16205–16209.
[86] C.S. Yee, M.C.Y. Chang, J. Ge, D.G. Nocera, J. Stubbe, 2,3-difluorotyrosine on R2 of ribonucleotide reductase: A probe of long-range proton-coupled electron transfer, J. Am. Chem. Soc. 125 (2003) 10506–10507.
[87] C.S. Yee, M.R. Seyedsayamdost, M.C.Y. Chang, D.G. Nocera, J. Stubbe, Generation of the R2 subunit of ribonucleotide reductase by intein chemistry: insertion of 3-nitrotyrosine at residue 356 as a probe of the radical initiation process, Biochemistry 42 (2003) 14541–14552.
[88] C.K. Chang, I. Abdalmuhdi, Anthracene pillared cofacial porphyrins, J. Org. Chem. 48 (1983) 5388–5390.
[89] C.K. Chang, I. Abdalmuhdi, A biphenylenediporphyrin — two cofacially arranged porphyrins with a biphenylene bridge, Angew. Chem., Int. Ed. Engl. 23 (1984) 164–165.
[90] J.P. Collman, J.E. Hutchison, M.A. Lopez, A. Tabard, R. Guilard, W.K. Seok, J.A. Ibers, M. L'Her, Synthesis and characterization of a superoxo complex of the dicobalt cofacial diporphyrin [(μ-O_2)Co_2(DPB)(1,5-diphenylimidazole)$_2$]PF_6, the structure of the parent dicobalt diporphyrin Co_2(DPB), and a new synthesis of the free-base cofacial diporphyrin H_4(DPB), J. Am. Chem. Soc. 114 (1992) 9869–9877.
[91] J.P. Collman, P.S. Wagenknecht, J.E. Hutchison, Molecular catalysts for multielectron redox reactions of small molecules — the cofacial metallodiporphyrin approach, Angew. Chem., Int. Ed. Engl. 33 (1994) 1537–1554.
[92] C.J. Chang, Y. Deng, A.F. Heyduk, C.K. Chang, D.G. Nocera, Xanthene-bridged cofacial bisporphyrins, Inorg. Chem. 39 (2000) 959–966.
[93] C.J. Chang, E.A. Baker, B.J. Pistorio, Y. Deng, Z.H. Loh, S.E. Miller, S.D. Carpenter, D.G. Nocera, Structural, spectroscopic and reactivity comparison of xanthene- and dibenzofuran-bridged cofacial bisporphyrins, Inorg. Chem. 41 (2002) 3102–3109.
[94] C.J. Chang, Y. Deng, S.M. Peng, G.H. Lee, C.Y. Yeh, D.G. Nocera, A convergent synthetic approach using sterically demanding aryldipyrrylmethanes for tuning the pocket sizes of cofacial bisporphyrins, Inorg. Chem. 41 (2002) 3008–3016.

[95] L.L. Chng, C.J. Chang, D.G. Nocera, Meso-tetraaryl cofacial bisporphyrins delivered by suzuki cross-coupling, J. Org. Chem. 68 (2003) 4075–4078.
[96] C.J. Chang, Z.H. Loh, Y. Deng, D.G. Nocera, The pacman effect: a supramolecular strategy for controlling the excited state dynamics of pillared cofacial bisporphyrins, Inorg. Chem 42 (2003) 8262–8267.
[97] C.J. Chang, Y. Deng, C. Shi, C.K. Chang, F.C. Anson, D.G. Nocera, Electrocatalytic four-electron reduction of oxygen to water by a highly flexible cofacial cobalt bisporphyrin, Chem. Commun., (2000) 1355–1356.
[98] Y. Deng, C.J. Chang, D.G. Nocera, Direct observation of the pacman effect from dibenzofuran-bridged cofacial bisporphyrins, J. Am. Chem. Soc. 122 (2000) 410–411.
[99] B.J. Pistorio, C.J. Chang, D.G. Nocera, A phototriggered molecular spring for aerobic catalytic oxidation reactions, J. Am. Chem. Soc. 124 (2002) 7884–7885.
[100] J.M. Hodgkiss, C.J. Chang, B.J. Pistorio, D.G. Nocera, Transient absorption studies of the pacman effect in spring-loaded diiron(III) μ-oxo bisporphyrins, Inorg. Chem. 42 (2003) 8270–8277.
[101] C.J. Chang, C.Y. Yeh, D.G. Nocera, Porphyrin architectures bearing functionalized xanthene spacers, J. Org. Chem. 67 (2002) 1403–1406.
[102] S.I. Ozaki, M.P. Roach, T. Matsui, Y. Watanabe, Investigations of the roles of the distal heme environment and the proximal heme iron ligand in peroxide activation by heme enzymes via molecular engineering of myoglobin, Acc. Chem. Res. 34 (2001) 818–825.
[103] A.R. Dunn, I.J. Dmochowski, A.M. Bilwes, H.B. Gray, B.R. Crane, Probing the open state of cytochrome P450cam with ruthenium-linker substrates, Proc. Natl. Acad. Sci. U. S. A. 98 (2001) 12420–12425.
[104] I. Hamachi, S. Tsukiji, S. Shinkai, S. Oishi, Direct observation of the ferric-porphyrin cation radical as an intermediate in the photo-triggered oxidation of ferric- to ferryl-heme tethered to $Ru(bpy)_3$ in reconstituted myoglobin, J. Am. Chem. Soc. 121 (1999) 5500–5506.
[105] C.Y. Yeh, C.J. Chang, D.G. Nocera, Hangman porphyrins for the assembly of a model heme water channel, J. Am. Chem. Soc. 123 (2001) 1513–1514.
[106] C.J. Chang, L.L. Chng, D.G. Nocera, Proton-coupled O–O activation on a redox platform bearing a hydrogen scaffold, J. Am. Chem. Soc. 125 (2003) 1866–1876.
[107] L.L. Chng, C.J. Chang, D.G. Nocera, Disproportionation of hydrogen peroxide catalyzed by iron hangman porphyrins with different proton-donating abilities, Org. Lett. 5 (2003) 2421–2424.
[108] R.I. Cukier, S.A. Seibold, Molecular dynamics simulations of prostaglandin endoperoxide H synthase-1. Role of water and the mechanism of compound I formation from hydrogen peroxide, J. Phys. Chem., B 106 (2002) 12031–12044.
[109] Y. Watanabe, High-valent intermediates, in: K.M. Kadish, K.M. Smith, R. Guilard (Eds.), The Porphyrin Handbook, vol. 4. Academic Press, San Diego, 2000, pp. 97–117.
[110] N.C. Veitch, A.T. Smith, Horseradish peroxidase, Adv. Inorg. Chem. 51 (2001) 107–162.
[111] H.B. Dunford, Heme Peroxidases, Wiley, New York, 1999.
[112] T.M. Makris, R. Davydov, I.G. Denisov, B.M. Hoffman, S.G. Sligar, Mechanistic enzymology of oxygen activation by the cytochromes P450, Drug Metab. Rev. 34 (2002) 691–708.
[113] C.E. MacBeth, A.P. Golombek , V.G. Young Jr., C. Tang, K. Kuczera, M.P. Hendrich, A.S. Borovik, O_2 activation by non-heme iron complexes: a monomeric Fe(III)-oxo complex derived from O_2, Science 289 (2000) 938–941.
[114] A. Wada, S. Ogo, S. Nagatomo, T. Kitagawa, Y. Watanbe, K. Jitsukawa, H. Masuda, Reactivity of hydroperoxide bound to a mononuclear non-heme iron site, Inorg. Chem. 41 (2002) 616–618.
[115] J. Feitelson, E. Hayon, Electron ejection and electron capture by phenolic compounds, J. Phys. Chem. 77 (1973) 10–15.